# Raman scattering study of β-$Sr_{0.33}V_2O_5$ in charge disordered and ordered phase



2006 J. Phys.: Condens. Matter 18 7779

(http://iopscience.iop.org/0953-8984/18/32/024)

INSTITUTE OF PHYSICS PUBLISHING JOURNAL OF PHYSICS: CONDENSED MATTER

J. Phys.: Condens. Matter **18** (2006) 7779–7787 doi:10.1088/0953-8984/18/32/024

# Raman scattering study of $\beta$-$Sr_{0.33}V_2O_5$ in charge disordered and ordered phase

**Z V Popović[1], A G Kontos[2], Y S Raptis[2], M Isobe[3] and Y Ueda[3]**

[1] Center for Solid State Physics and New Materials, Institute of Physics, Pregrevica 118, 11080 Belgrade, Serbia
[2] Physics Department, National Technical University of Athens, GR 157 80 Athens, Greece
[3] Materials Design and Characterization Laboratory, Institute for Solid State Physics, The University of Tokyo, 5-1-5 Kashiwanoha, Kashiwa, Chiba 277-8581, Japan

Received 14 April 2006, in final form 19 June 2006
Published 31 July 2006
Online at stacks.iop.org/JPhysCM/18/7779

**Abstract**

Polarized Raman spectra of the strontium vanadium oxide bronze $\beta$-$Sr_{0.33}V_2O_5$ are measured in the temperature range between 300 and 77 K. The charge ordering phase transition at about 165 K is characterized by the appearance of new Raman-active modes in the spectra, as well as through an abrupt change of the phonon frequencies and dampings. The Raman scattering spectra of $\beta$-$Sr_{0.33}V_2O_5$ in the charge disordered phase are in apparent resemblance with those of $\alpha'$-$NaV_2O_5$, which suggests that there is a similar charge-phonon dynamics in both compounds. We also suggest that the electrons are delocalized into $V_1$–$O_5$–$V_3$ orbitals in the mixed valence state of $\beta$-$Sr_{0.33}V_2O_5$.

(Some figures in this article are in colour only in the electronic version)

## 1. Introduction

The vanadium bronzes, $\beta(\beta')$-$A_x^{1+(2+)}V_2O_5$ ($x = \frac{1}{3}, \frac{2}{3}$; A = Li, Na, Ag, Ca, Sr, Pb, Cu etc) exhibit a variety of phenomena that originate from strong electron correlations. For example, various charge and spin orderings [1–4], and even superconductivity ($\beta$-$Na_{0.33}V_2O_5$ [5] and $\beta'$-$Cu_{0.65}V_2O_5$ [6]) are found in this class of materials. These findings renewed the interest in low-dimensional vanadium oxides [7–9]. The different phases of the $\beta$-$A_{0.33}V_2O_5$ family, also referred to as $\beta$-$AV_6O_{15}$, exhibit one-dimensional metallic behaviour at room temperature and undergo a metal-to-insulator phase transition at $T_{MI}$, associated with a charge ordering. Systems with monovalent cations ($A^+$) show long-range magnetic order at $T < T_{MI}$. In systems with divalent cations ($A^{2+}$), no sign of long-range magnetic order is observed down to 2 K and a spin gap appears in $SrV_6O_{15}$ [2].

The electronic properties of $\beta$-$SrV_6O_{15}$ are discussed in [9]. Spin dimer analysis, based on extended Hückel tight-binding calculations, was performed to determine the structure of the dominant transfer and magnetic interactions in the room-temperature $\beta$-$SrV_6O_{15}$ phase.

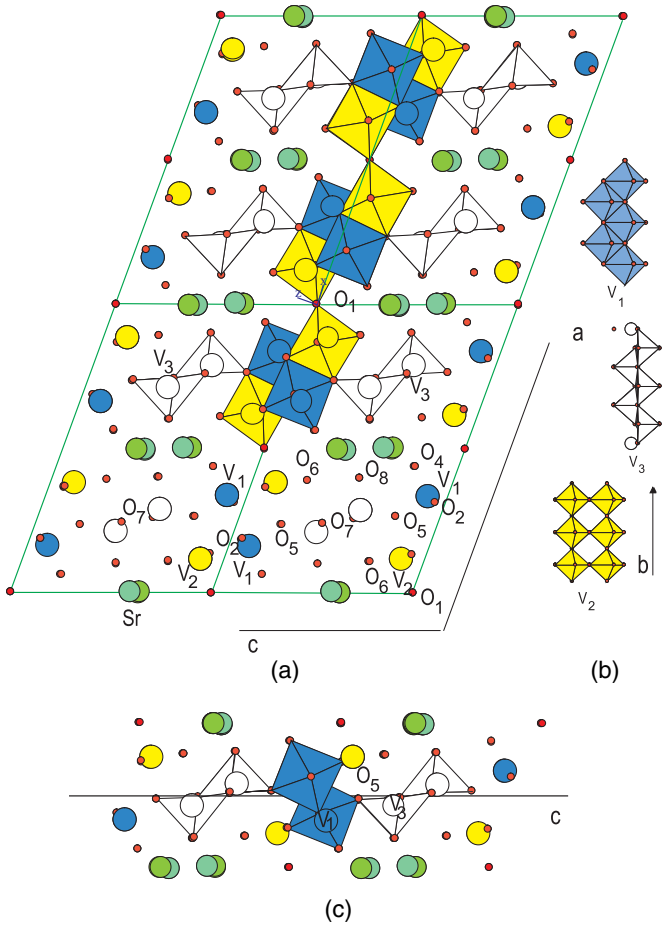


**Figure 1.** (a) Crystal structure of $\beta$-$Sr_{0.33}V_2O_5$ projected on the ($ac$) plane. (b) Three types of V-chains running parallel to the $b$-axis. (c) Schematic representation of the up-up–down-down orientation of the $VO_5$ and $VO_6$ polyhedra along the $c$-axis.

According to these calculations, the dominant interactions are arranged in two types of two-leg ladders (the $V_2$–$V_2$ and the $V_1$–$V_3$ ladders), which are crystallographically orthogonal to each other. All magnetic interactions within these ladders show an antiferromagnetic character [9].

The $\beta$ compounds with divalent A cations such as $Ca^{2+}$ and $Sr^{2+}$ were first prepared by Bouloux *et al* [10]. The room-temperature crystal structure of the $\beta$-phase was initially described as monoclinic, space group $C2/m$ ($C^3_{2h}$) with $Z = 6$ formula units per unit cell [11]. It has a characteristic $V_2O_5$ framework formed by the edge/corner shearing $VO_5$ and $VO_6$, as shown in figure 1. There are three different sites for vanadium atoms: $V_1$, $V_2$ and $V_3$. The $V_2O_5$ framework consists of three kinds of infinite double chains along the $b$-axis, as shown in figure 1(b). The $V_1$ sites have six-fold, octahedral coordination and form a zigzag chain by sharing the edges of the $VO_6$ octahedra. The $V_2$ sites with similar octahedral coordination form a ladder chain by sharing corners, and the $V_3$ sites, which have five-fold square pyramidal coordination, form a zigzag chain by sharing the edges. The Sr cations are located at the sites in the tunnel formed by the $V_2O_5$ framework. Recently, the x-ray measurements [12, 13]

revealed the presence of a superstructure with a lattice modulation vector $\vec{q} = (0, 1/2, 0)$ at room temperature in $\beta$-$Sr_{0.33}V_2O_5$. This indicates the doubling of the unit cell along the $b$-axis. The diffraction pattern of this phase has been indexed using the $P2_1/a$ space group and the following unit cell parameters: $a = 15.4356$ Å, $b = 7.3025$ Å, $c = 10.1632$ Å, $\beta = 109.41°$, and $Z = 4$ [12, 13]. Such a superstructure was also observed in $\beta$-$A^{1+}_{0.33}V_2O_5$ (A = Na and Ag) [14] below room temperature originating from the ordering of the A cations along the $b$-axis, which is a formation of the A-chains where the A cations and vacancies alternate with each other.

The magnetic susceptibility of $\beta$-$Sr_{0.33}V_2O_5$ versus temperature shows a slight jump at around 168 K [14] indicating the existence of a phase transition. Above the transition temperature, the magnetic susceptibility is almost temperature independent, whereas below the transition temperature it shows a low-dimensional behaviour. The magnetic susceptibility has a maximum at around 50 K, then further decreases by reducing the temperature, with an upturn at lower temperatures which is caused by the impurities or defects [14]. At the phase transition the lattice parameters show a discontinuous change that is typical for a first-order transition. The NMR study [15] has revealed that above ∼165 K there is only one kind of electronic state of the V site, whereas below this temperature one finds two kinds of V sites, which can be identified as magnetic $V^{4+}$ and nonmagnetic $V^{5+}$. This finding strongly suggests the existence of a charge ordering (CO) transition or the appearance of a charge disproportion at $T_{CO} \sim 165$ K.

Here we analyse Raman scattering spectra above and below the charge ordering phase transition in $\beta$-$Sr_{0.33}V_2O_5$. The appearance of new Raman modes in the charge ordered phase as well as an abrupt change of phonon frequency and damping show that the phase transition has a strong influence on the phonon dynamics of $\beta$-$Sr_{0.33}V_2O_5$.

## 2. Experiment

Single crystals of $\beta$-$Sr_{0.33}V_2O_5$ were grown by a flux method using $SrV_2O_6$ as a flux. $SrV_2O_6$ was prepared by a solid-state reaction between $SrCO_3$ and $V_2O_5$ in air at 600 °C. Details of the sample preparation were published in [6]. The Raman spectra were measured from small crystals of typical size 0.1–0.5 mm along the $b$-direction and about 0.01–0.05 mm in the other two directions. Polarized spectra have been measured in a backscattering geometry using a micro-Raman system with a Jobin Yvon T64000 triple monochromator including a liquid nitrogen cooled charge-coupled-device (CCD) detector. The 514.5 nm line of an Ar-ion laser was used as an excitation source. Low-temperature measurements were carried out in an Oxford Instruments continuous flow cryostat with a 0.5 mm thick window. The laser beam was focused by a long-distance (3.5 mm focal length) microscope objective (magnification 100×). The spectra were calibrated by recording the emission spectrum of a Hg lamp before and after completing a set of spectra at a specific temperature. We have measured low-excitation-power (0.3 mW) spectra at low temperatures (∼80 K) in order to minimize laser-induced heating effects (frequency shifts, line broadenings, and band overlap). For the consequent spectra at variable temperatures, we have used an excitation power of 1 mW in order to obtain an acceptable signal/noise ratio with reasonable acquisition times. This power increase (and the resulting band broadening) does not alter significantly the manifestation of the temperature effects investigated. However, the actual temperature of the scattering volume is estimated to be ∼15–20 K higher than the nominal $T$-value. 1. To get rid of the trivial temperature dependence, all spectra have been divided by the Bose–Einstein occupation number, $n(\omega) + 1 = 1/[1 - \exp(-\hbar\omega/k_B T)]$.

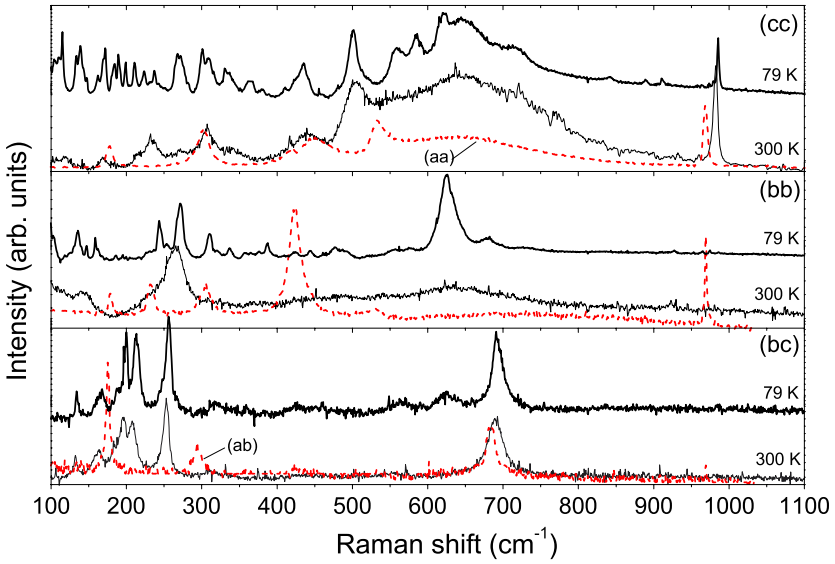


**Figure 2.** Room-temperature and liquid-nitrogen temperature polarized Raman spectra of $\beta$-$Sr_{0.33}V_2O_5$, together with corresponding roo-temperature Raman spectra of $\alpha'$-$NaV_2O_5$ (dashed lines). $\lambda_L = 514.5$ nm.

## 3. Results and discussion

At room temperature the $SrV_6O_{15}$ unit cell consists of four formula units ($Z = 4$) with 88 atoms in all. Due to the low symmetry and the large number of atoms in the unit cell, we can expect a large number of optically active modes. All atoms have $4(e)$ position symmetry of $P2_1/c(C_{2h}^5)$ space group [13]. Factor group analysis (FGA) yields the following distribution of vibrational modes:

$$\Gamma = 66A_g(xx, yy, zz, xz) + 66B_g(xy, yz) + 66A_u(\mathbf{E} \parallel \mathbf{y}) + 66B_u(\mathbf{E} \perp \mathbf{y}).$$

According to this representation, one can expect 132 Raman and 129 infrared active modes ($1A_u + 2B_u$ are acoustic modes).

The polarized Raman spectra of $\beta$-$Sr_{0.33}V_2O_5$, measured from the (bc) plane at room-temperature and liquid-nitrogen temperature are given in figure 2 together with the polarized Raman spectra of $\alpha'$-$NaV_2O_5$. At a first glance, we found that the number of observed modes is much less than the FGA predicted. Namely, only 20 modes are observed at room temperature for parallel polarization ($A_g$ symmetry modes) and only seven for crossed polarization ($B_g$ symmetry modes); see table 1. Further, almost all of the observed modes have a large width. This strong broadening is due to a strong electron–phonon coupling and/or near degeneracy of many modes with nearly the same energies. Finally, we have found that these spectra coincide with $\alpha'$-$NaV_2O_5$ in many details, which suggests structural similarities and similarities in the normal coordinates of their vibrational modes. Exploiting ths by carefully fitting the low-excitation power (0.3 mW) spectra at 79 K using the Lorentzian deconvolution technique, we can reveal a significantly larger number of definite peaks. The mode frequencies given in table 1 were obtained as a result of such a procedure.

As was already discussed in the case of $AV_2O_5$ [16], the phonon modes in the spectral range below 500 $cm^{-1}$ originate from the bond-bending vibrations, whereas the higher-frequency modes originate from the stretching vibrations of the V–O ions. The highest-

**Table 1.** Frequencies (in $cm^{-1}$) of Raman-active modes of $\beta$-$Sr_{0.33}V_2O_5$.

| 300 K | | 79 K | | |
|---|---|---|---|---|
| $A_g$ | $B_g$ | $A_g$ | | $B_g$ |
| 61.5 | 133.0 | 58.2 | 282.0 | 57.9 |
| 95.4 | 164.2 | 64.3 | 300.6 | 64.4 |
| 96.7 | 196.6 | 70.7 | 310.0 | 133.0 |
| 107.0 | 207.0 | 76.3 | 321.8 | 138.1 |
| 118.6 | 252.7 | 80.0 | 330.8 | 153.8 |
| 142.7 | 310.1 | 89.3 | 336.0 | 161.7 |
| 168.0 | 686.6 | 95.7 | 358.9 | 167.2 |
| 184.5 | | 99.3 | 363.7 | 187.0 |
| 215.6 | | 104.6 | 376.1 | 199.0 |
| 234.5 | | 110.0 | 380.4 | 212.0 |
| 265.4 | | 115.0 | 387.5 | 242.9 |
| 271.0 | | 133.5 | 410.4 | 248.0 |
| 307.1 | | 139.0 | 423.0 | 255.0 |
| 339.0 | | 143.0 | 435.0 | 267.8 |
| 416.9 | | 147.5 | 442.2 | 317.0 |
| 444.0 | | 158.8 | 477.2 | 359.8 |
| 506.0 | | 162.0 | 492.4 | 382.1 |
| 641.4 | | 169.0 | 500.2 | 425.7 |
| 922.0 | | 172.0 | 559.5 | 564.0 |
| 981.5 | | 180.0 | 577.2 | 624.2 |
| | | 184.4 | 585.2 | 692.0 |
| | | 189.1 | 624.0 | |
| | | 195.3 | 632.2 | |
| | | 199.0 | 646.0 | |
| | | 210.9 | 679.7 | |
| | | 223.6 | 713.7 | |
| | | 229.5 | 730.5 | |
| | | 237.2 | 841.0 | |
| | | 244.0 | 890.0 | |
| | | 264.0 | 911.0 | |
| | | 268.0 | 922.0 | |
| | | 271.0 | 985.6 | |
| | | 276.6 | | |

frequency mode at 985.6 $cm^{-1}$ (79 K) represents $V_3$–$O_8$ (see figure 1) stretching vibrations (the V–$O_1$ bond stretching vibration in sodium vanadate [16]), whereas the modes at about 890 and 911 $cm^{-1}$ originate from $V_2$–$O_6$ and $V_1$–$O_4$ bond stretching vibrations, respectively. These modes appear at the highest frequencies, because they are coming from the shortest-distance V–O bonds (the $V_3$–$O_8$ bond in the $VO_5$ pyramid, and the $V_2$–$O_6$ and $V_1$–$O_4$ bonds in the $VO_6$ octahedra; see figure 1). Note that the V–O bond-stretching vibrational modes in the octahedral surrounding have lower frequencies than in the pyramidal one, as it is already found in [17].

The $B_g$ symmetry mode at 692 $cm^{-1}$ (79 K) corresponds to the bond stretching vibrations of $V_3$ and $O_7$ ions along the *b*-axis. Since the $V_3$–$O_7$ distance in $\beta$-$Sr_{0.33}V_2O_5$ is close to the corresponding distance V–$O_{2b}$ in $\alpha'$-$NaV_2O_5$, there is no significant mode frequency difference between these two oxides. The next $A_g$ mode of $\beta$-$Sr_{0.33}V_2O_5$ appears at a frequency of 500.2 $cm^{-1}$ (at low-*T*) or 506 $cm^{-1}$ (at room-*T*). The frequency of the analogous mode in $\alpha'$-$NaV_2O_5$ is 534 $cm^{-1}$. This mode represents the bond-stretching vibration of $V_3$ and $O_7$ ions, along the *c*-axis. The frequency difference between these modes is in accordance with the

difference between values of the $V_3$–$O_{7c}$ bond lengths in $\beta$-$Sr_{0.33}V_2O_5$ (2.0 Å) and V–$O_{2a}$ in $\alpha'$-$NaV_2O_5$ (1.985 Å).

The Raman mode at 448 $cm^{-1}$ in $\alpha'$-$NaV_2O_5$ is related to the V–$O_3$–V bending vibrations [16] (mostly the vibration of oxygen ions in the rungs of the ladder structure of sodium vanadate along the $c$-axis direction). As we discussed in [16, 18], the force constant of this mode is strongly affected by the charge of the electrons in the rung. Because of that, this mode appears at a frequency below its intrinsic value of 485 $cm^{-1}$ in pure $V_2O_5$ or 470 $cm^{-1}$ in $CaV_2O_5$ (where spin electrons are attached to the $V^{4+}$ ions) [16]. In addition, this mode in $\alpha'$-$NaV_2O_5$ shows strong asymmetry and broadening. Since this mode has the same shape and position in both $\alpha'$-$NaV_2O_5$ and $\beta$-$Sr_{0.33}V_2O_5$ ($\sim$444 $cm^{-1}$ at RT; 435 $cm^{-1}$ at 79 K), we suggest that the electrons in $\beta$-Sr vanadate bronze are also delocalized in the V–O–V orbitals, where the O denotes common corner oxygen ions between the $VO_{5(6)}$ polyhedra. There are two bridge oxygens in different $VO_{5(6)}$ polyhedra: $O_1$ and $O_5$ (figure 1). Since the $O_1$ atom in the $C2/m$ average structure is in the centre of inversion, its vibration does not contribute to the Raman scattering process. In the case of $P2_1/a$ symmetry, this oxygen could participate in the Raman scattering process, but the $V_2$–$O_1$–$V_2$ bond length (3.624 Å) and bond angle (176°) are far from the corresponding V–O–V values in sodium vanadate. Thus, we concluded that only the $O_5$ ion vibration can be included in the normal coordinate of the 444 $cm^{-1}$ V–O–V bond-bending mode. Furthermore, there are six possible V–$O_{5a,5b}$–V bonds for the normal coordinate of the 444 $cm^{-1}$ mode: $V_{2a,2b}$–$O_{5a,5b}$–$V_{1a,1b}$, $V_{2a,2b}$–$O_{5a,5b}$–$V_{3a,3b}$ and $V_{1a,1b}$–$O_{5a,5b}$–$V_{3a,3b}$. Since only the $V_{1a,1b}$–$O_{5a,5b}$–$V_{3a,3b}$ bond has nearly the same bond length (3.74 Å) and bond angle (136°) as in $\alpha'$-$NaV_2O_5$ [16], we deduce that the 444 $cm^{-1}$ mode corresponds to the $V_1$–$O_5$–$V_3$ bond-bending vibration. This means that, although $V_1$ and $V_3$ are different site V ions, they are in the mixed valence state ($V^{4.5+}$), whereas $V_2$ can be all in 5+ states at room temperature. Recent calculations [9] of leading interactions in $\beta$-$Sr_{0.33}V_2O_5$ show the existence of strong charge transfer in the rung of $V_1$–$V_3$ ladders too. This strongly supports our findings that the 444 $cm^{-1}$ mode is affected by the charge of the electrons in the $V_1$–$O_5$–$V_3$ rungs. The crystallographic similarity between $\alpha'$-$NaV_2O_5$ and $\beta$-$Sr_{0.33}V_2O_5$ is illustrated in figure 1(c). Note that the $VO_5$ pyramids and $VO_6$ octahedra are oriented along the $c$-axis in an 'up-up–down-down' pattern in $\beta$-$Sr_{0.33}V_2O_5$, similar to the $VO_5$ pyramidal structure along the $a$-axis in $\alpha'$-$NaV_2O_5$.

Below the charge ordering transition the unit cell triples, keeping the same symmetry ($P2_1/a$) [13]. In this case, the number of active phonons is 198 for each irreducible representation. At liquid-nitrogen temperature (figure 2) almost all modes split as a consequence of charge ordering followed by the tripling of the unit cell. Several modes also appear from the broad structure ranging from 550 up to 700 $cm^{-1}$; see figure 3. The localization of the electrons leads to a decrease in the coupling of these phonons to electronic excitations, and they become more pronounced below the transition temperature (150 K). At the lowest temperature used in our experiments (80 K), these modes are the most intense ones, though they are much broader than the rest of them.

Concerning the ($cc$) polarized spectra (figure 3) with the temperature decrease, the appearance of several new modes in the spectral range below 400 $cm^{-1}$ is observed, as well as the decomposition of a broad band into five modes between 530 and 720 $cm^{-1}$ below 160 K. The frequencies of these modes are given in table 1. The most interesting effect for this polarization configuration is the softening of many Raman lines with the temperature decrease. In the inset of figure 3 we present the frequency versus temperature dependence of the 444 and 506 $cm^{-1}$ modes. These modes show remarkable mode softening (indicated also by the vertical lines in figure 3) as a consequence of the electron–phonon interaction reduction by phase transition from charge disordered to charge ordered state.

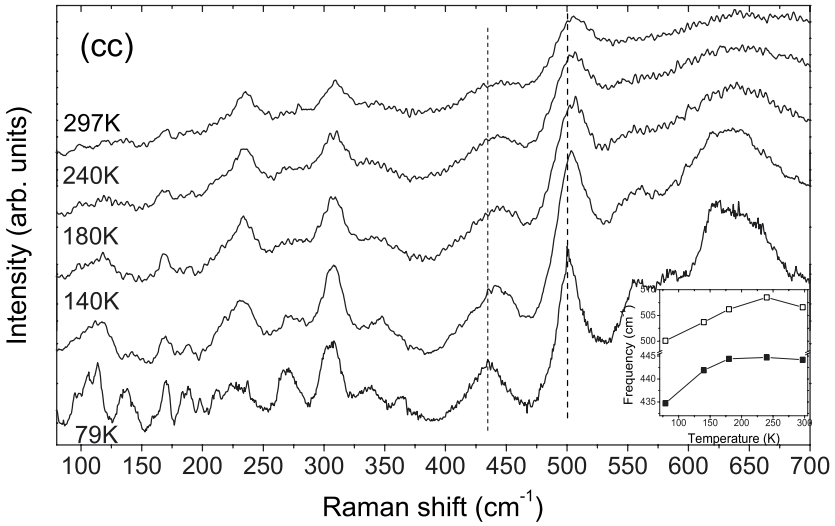


**Figure 3.** The (*cc*) polarized Raman spectra of $\beta$-$Sr_{0.33}V_2O_5$ at different temperatures. Inset: the frequency versus temperature dependence of the 444 and 506 $cm^{-1}$ modes.

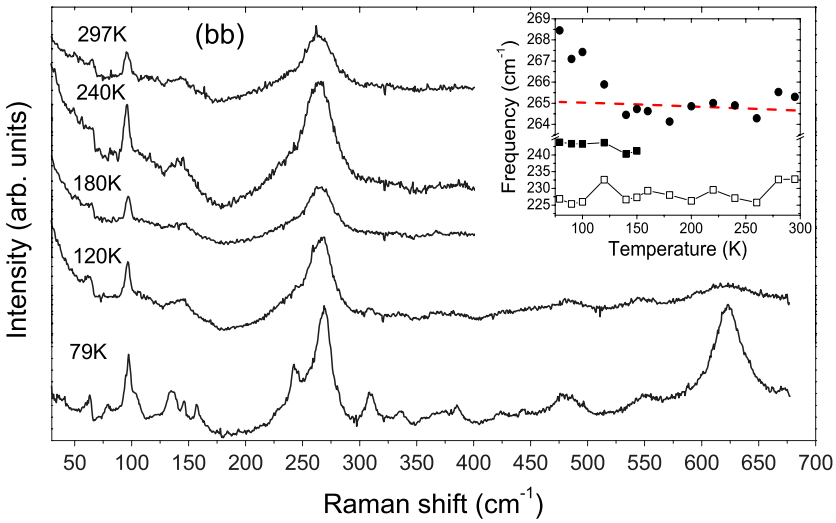


**Figure 4.** The (*bb*) polarized Raman spectra of $\beta$-$Sr_{0.33}V_2O_5$ at different temperatures. Inset: frequency versus temperature dependence of the 232, 244 and 265 $cm^{-1}$ modes. The dashed line represents the anharmonic phonon–phonon interaction spectrum (see text). The laser excitation wavelength was 514.5 nm.

Raman spectra for the (bb) polarization are shown in figure 4. The sharp line at about 97 $cm^{-1}$ (80 K) preserves its characteristics over the whole temperature range. Two other characteristic features of the same polarization configuration, related to the frequency range of 200–300 $cm^{-1}$ and the well-defined band peaked at 624 $cm^{-1}$, demonstrate the existence of a transition temperature at around 160 K. For the latter, a fast broadening is observed with the temperature increase followed by a gradual decrease in the integrated intensity and a slight

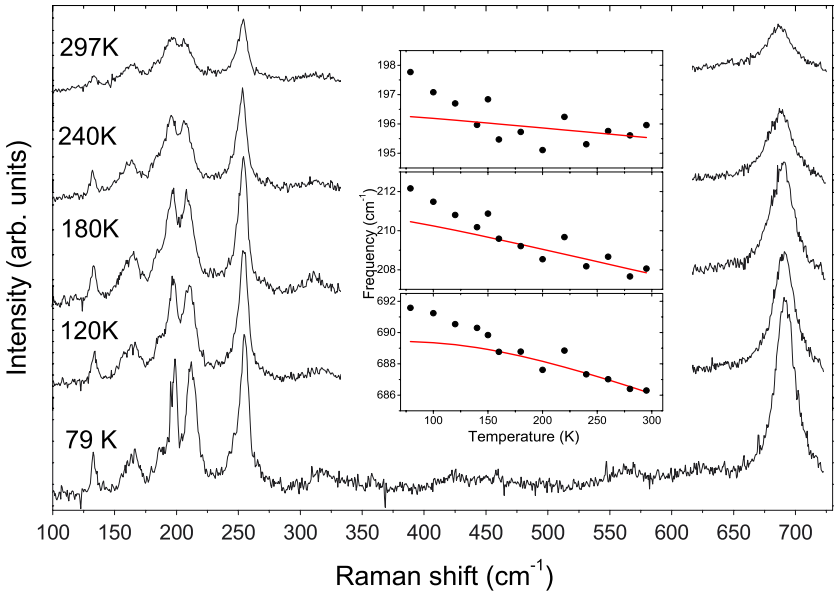


**Figure 5.** The (*bc*) polarized Raman spectra of $\beta$-$Sr_{0.33}V_2O_5$ at different temperatures. Inset: frequency versus temperature dependence of the 196, 208 and 686 $cm^{-1}$ modes. The solid lines represent the anharmonic phonon–phonon interaction spectra calculated with the following parameters (in $cm^{-1}$): $\omega_0 = 196.6$, $C = -0.25$; $\omega_0 = 211.8$, $C = -1.0$; and $\omega_0 = 696.7$, $C = -7.25$; for 196, 208 and 686 $cm^{-1}$ modes, respectively. The laser excitation wavelength was 514.5 nm.

softening; this peak is not observed above 160 K. The former range consists of three peaks, whose frequency versus temperature dependences are shown in the inset of figure 4. The mode at 234 $cm^{-1}$ shows a slight softening below the phase transition due to repulsion with the new mode, which appears at about 244 $cm^{-1}$ below 150 K. The highest-frequency mode in this spectral range (265.4 $cm^{-1}$ at RT) shows a steep frequency change at about 150 K. In order to distinguish the phonon–phonon contribution due to the anharmonic effects from the charge-ordering-related contribution, we have fitted the high-temperature part (160–300 K) of the frequency versus temperature dependence using a model for the anharmonic phonon–phonon interaction [19]:

$$\omega_{ph}(T) = \omega_0 + C[1 + 2/(e^{\omega_0/2kT} - 1)], \tag{1}$$

where $\omega_0$ and $C$ have the values 265.4 and $-0.25$ $cm^{-1}$. The calculated spectrum is represented by a dashed line in the inset of figure 4. It is obvious that the dominant contribution in the frequency versus temperature dependence of the 265 $cm^{-1}$ mode below the phase transition arises from lattice and charge rearrangement but not from phonon–phonon scattering due to anharmonic effects.

The $B_g$ symmetry modes, obtained through the (*bc*) polarization combination, are presented in figure 5. Contrary to the $A_g$ modes, the $B_g$ symmetry modes do not change significantly with the temperature increase, maintaining nearly constant absolute and relative (with respect to each other) intensities. However, considering the frequency shifts of 196.6, 207 and 686.6 $cm^{-1}$ modes as a function of temperature (the inset of figure 5), using the anharmonic model, equation (1), we found that the phase transition leaves a fingerprint in the phonon dynamics of $\beta$-$Sr_{0.33}V_2O_5$. The 686.6 $cm^{-1}$ mode is isolated, which means that it does

not couple with surrounding Raman modes in the low-temperature phase. The frequency of the mode increases monotonously from room temperature to the phase transition temperature, where a change in frequency is observed. The frequency variation is a consequence of the change in the crystal and magnetic structure at the phase transition due to the charge ordering.

In conclusion, the Raman scattering spectra of $\beta$-$Sr_{0.33}V_2O_5$ are studied from liquid-nitrogen temperature up to room temperature. By monitoring the temperature dependence for several Raman features of the three different polarization combinations, the existence of a transition at about 165 K was confirmed. Similarities in the phononic and electronic excitations, between $\beta$-$Sr_{0.33}V_2O_5$ and $\alpha'$-$NaV_2O_5$, were discussed in terms of a charge ordering occurring below the transition temperature. At temperatures above the phase transition temperature the broadening and the asymmetry of the 444 $cm^{-1}$ mode suggest that the electrons are delocalized into the $V_1$–$O_5$–$V_3$ orbitals. Below the phase transition, the charge ordering takes place, followed by the appearance of new Raman modes due to a tripling of the unit cell and decoupling of the phonons and electronic excitations. Analysing the phonon frequency and damping versus temperature, we found that the phase transition leaves a fingerprint in the phonon dynamics of $\beta$-$Sr_{0.33}V_2O_5$.

## Acknowledgment

This work is supported by the bilateral Greek–Serbian collaboration 'Joint Research and Technology Programmes, 2003–2005'.

## References

[1] Yamada H and Ueda Y 1999 *J. Phys. Soc. Japan* **68** 2735
Yamada H and Ueda Y 2000 *J. Phys. Soc. Japan* **69** 1437
[2] Ueda Y, Yamada H, Isobe M and Yamauchi T 2001 *J. Alloys Compounds* **317/318** 109
[3] Obermeier G, Ciesla D, Klimm S and Horn S 2002 *Phys. Rev.* B **66** 085117
[4] Vasil'ev A N, Marchenko V I, Smirnov A I, Sosin S S, Yamada H and Ueda Y 2002 *Phys. Rev.* B **64** 174403
[5] Yamauchi T, Ueda Y and Mori N 2002 *Phys. Rev. Lett.* **89** 057002
[6] Ueda Y, Isobe M and Yamauchi T 2002 *J. Phys. Chem. Solids* **63** 951
[7] Presura C, Popinciuc M, van Loosdrecht P H M, van der Marel D, Mostovoy M, Yamauchi T and Ueda Y 2003 *Phys. Rev. Lett.* **90** 026402
[8] Heinrich M, Krug von Nidda H-A, Eremina R M, Loidl A, Helbig Ch, Obermeier G and Horn S 2004 *Phys. Rev. Lett.* **93** 116402
[9] Doublet M-L and Lepetit M-B 2005 *Phys. Rev.* B **71** 075119
[10] Bouloux J C, Galy J and Hagenmuller P 1974 *Rev. Chim. Mineral.* **11** 48
[11] Déramond E, Savariault J M and Galy J 1994 *Acta Crystallogr.* C **50** 164
[12] Yamura J I, Isobe M, Yamada H, Yamauchi T and Ueda Y 2002 *J. Phys. Chem. Solids* **63** 957
[13] Sallier C, Boucher F and Junod E 2003 *Solid State Sci.* **5** 591
[14] Isobe M and Ueda Y 2000 *Mol. Cryst. Liq. Cryst.* **341** 1075
[15] Itoh M, Akimoto N, Tsuchiya M, Yamada H, Isobe M and Ueda Y 2000 *Physica* B **281/282** 606
Itoh M, Akimoto N, Yamada H, Isobe M and Ueda Y 2001 *J. Phys. Chem. Solids* **62** 351
[16] Popović Z V, Konstantinović M J, Gajić R, Popov V N, Isobe M, Ueda Y and Moshchalkov V V 2002 *Phys. Rev.* B **65** 184303
[17] Loa I, Schwarz U, Hanfland M, Kremer R K and Syassen K 1999 *Phys. Status Solidi* b **215** 709
[18] Konstantinović M J, Popović Z V, Moshchalkov V V, Presura C, Gajić R, Isobe M and Ueda Y 2002 *Phys. Rev.* B **65** 245103
[19] Balkanski M, Wallis R F and Haro E 1983 *Phys. Rev.* B **28** 1928